

**Section 1**  
**Chapter**

## Imaging techniques

# The future of imaging and assisted reproduction

Alan H. DeCherney and Micah J. Hill

### Introduction

The clinician has many tools in evaluating the patient with diseases of the reproductive tract: patient history, a thorough examination, an array of serum tests, and several imaging studies. In order to obtain and interpret the appropriate tests, the clinician requires a basic understanding of how each radiologic modality functions and which test will best serve the patient. An intimate knowledge of the anatomy is required to appropriately interpret and apply the results of the test. This chapter reviews the basic principles of radiologic tests, reviews basic female anatomy, and provides information for appropriate imaging modalities for each part of the female genital tract.

### Technology

Radiographs comprise the majority of radiologic examinations, although they are used less frequently in evaluating the female genital tract. Radiographic examinations are performed by passing x-ray beams through the patient and detecting them on film or with detectors. These beams are either absorbed or scattered, depending on the type of tissue the radiation is passing through. Air and water typically show as black on the film. Bone and calcium deposits appear white. Fat and muscle appear as a faded white or gray color. Contrast agents also typically appear white. Radiographs provide only a two-dimensional view of tissue, often necessitating multiple films from multiple angles to provide a three-dimensional impression.

An extension of x-ray imaging used in reproductive medicine is hysterosalpingography (HSG). As the internal anatomy of the pelvis is primarily soft tissue, it appears black or gray on regular x-ray film. HSG utilizes a steady stream of x-rays (fluoroscopy) to capture images of the pelvis. As contrast material is injected into the uterus, a stream of images captures the contrast material, which reflects the internal anatomy of the uterus and fallopian tubes. HSG was initially described by Rindfleisch in 1910 [1] when early testing was performed with oil-soluble media. As this was accompanied by the risk of oil embolus and granuloma formation, water-soluble contrast materials are more commonly used today.

Computed tomography (CT) is performed using a rotating beam of x-rays which pass through the patient. The transmitted

x-rays are measured at thousands of points and a computer then creates an image based upon these data. A helical or spiral CT moves the x-ray tube and moves the patient table at the same time. The colors displayed in a CT image are similar to those on plain radiographs: air shows black, bone and contrast materials show white, and fat shows dark gray while soft tissue shows a lighter gray. CT scans present the images as “slices” or transverse two-dimensional images of the body. In CT imaging the density of tissue or fluid can be expressed using Hounsfield units.

Magnetic resonance imaging (MRI) is obtained by applying magnetic fields to the body. As the magnetic field passes through tissue, the intrinsic spins of hydrogen protons, initially randomly directed, are aligned with the field. Different radio-frequency pulses are then generated by the machine; the hydrogen protons absorb the energy as their spin “flips” to align against the direction of the applied magnetic field. This phenomenon is the resonance part of MRI. When the radio-frequency pulse is turned off, the hydrogen protons return to their natural alignment and energy is released. This produces a signal that is picked up by the coils and transmitted to a computer, which in turn uses the data to generate an image. MRI gradient magnets can be turned on and off in a very specific manner to target the tissue being imaged. MRI produces superior imaging of soft tissue and central nervous system tissue, but is poor for imaging bone and calcium. MRI can even be used to image the heart and blood vessels without the use of intravenous contrast. T1-weighted images produce images in which the fat is white and water is black. T2-weighted images show this reversed, with fat being dark and water being light. With both T1- and T2-weighted images, soft tissue appears gray in color.

Ultrasound images are produced by passing high-frequency sound waves through tissue and reading the echoes. The bladder or a fluid-filled cyst has few echoes and appears dark. Calcium and fat, on the other hand, reflect back high-intensity echoes and appear lighter. Advantages of ultrasound technology include real-time images and lack of ionizing radiation. Doppler modalities of ultrasound allow identification of the direction and magnitude of blood flow. More recently, three-dimensional ultrasound (3D US) has gained application in gynecology. Freehand 3D US images are obtained by manual

### Section 1: Imaging techniques

movement of the transducer through the region of interest, whereas automated 3D US images are obtained by holding the probe still while the transducer automatically sweeps through the area of interest. 3D US produces a variety of useful views of the organ being imaged, including multiplanar display, volume rendering, and surface rendering.

Positron emission tomography (PET) is unique in that it not only provides imaging of anatomical structures but can also give information on organ function. Small amounts of radiotracer are taken into the body by various routes (intravenous, inhalation, oral consumption) depending upon the organ being imaged. The tracer then gives off energy, which is detected by the PET scanner. Biologic function can be measured by this activity, including blood flow, oxygen consumption, and glucose metabolism.

## Uterus

No other reproductive organ involves more imaging tests than the uterus in reproductive medicine. From routine assessment of the cavity for infertility to disease states such as leiomyoma, adenomyosis, and müllerian anomalies, uterine imaging is essential to diagnosing reproductive disease. There are numerous imaging modalities well suited to evaluating the uterus, including conventional ultrasound, three-dimensional ultrasound, saline sonography, hysterosalpingography, magnetic resonance imaging, and computed tomography.

The inferiormost portion of the uterus is the cervix, which is mostly composed of fibrous tissue as opposed to the smooth muscle of the remainder of the uterus. The cervix is usually 2.5–3.5 cm in length and penetrates the vagina at the portio vaginalis. The body of the uterus is essentially a hollow muscular structure that consists of three layers similar to other visceral organs. The innermost layer is the endometrium, which functions as the implantation site for pregnancy. The middle layer, or myometrium, consists of interlacing smooth-muscle fibers and vascular channels. The outer layer is composed of visceral peritoneum and endopelvic fascia and covers the entire uterus with the exception of the vaginal portion of the cervix. The uterine blood supply comes from the uterine branch of the hypogastric artery. The vessels originate at the level of the cervix and course along the outer edge of the uterus up toward the fundus, where they anastomose with the ovarian vessels.

Imaging of the uterine cavity is typically performed with ultrasound technology, whether transvaginal (TVUS), transabdominal, or saline infusion sonography (SIS) or via hysterosalpingography (HSG). Infertility patients have a higher rate of cavitory lesions than patients with abnormal uterine bleeding. In a study of infertility patients, 20% were found to have a cavitory abnormality, including arcuate uterus (15%), polyps (13%), submucosal fibroids (3%), and adhesions (<1%) [2]. Traditional ultrasound may reveal abnormalities of the endometrium or uterine cavity as a thickened endometrial stripe. However, the sensitivity of transvaginal ultrasound in detecting cavitory abnormalities is low. Kelekci et al. showed that transvaginal sonography, SIS, and hysteroscopy had sensitivities and specificities of 56.3% and 72%, 81.3% and 100%, and 87.5% and 100% respectively for detecting cavitory lesions [3].



**Figure 1.1.** Transvaginal ultrasound showing a 22 mm endometrial stripe.



**Figure 1.2.** Hysteroscopic view of the uterus imaged in Figure 1.1 revealing the TVUS abnormality to be a uterine polyp.

Figure 1.1 shows a transvaginal ultrasound image exhibiting a thickened endometrial stripe of 22 mm. The differential diagnosis on this patient included an endometrial polyp and endometrial hyperplasia. Hysteroscopy (Figure 1.2) revealed an endometrial polyp with complex hyperplasia. While TVUS detected an abnormality, it was unable to provide specificity to the diagnosis. However, the ability of TVUS to suggest that an abnormality was present led to the confirmatory test and treatment, in this case hysteroscopy. Removal of endometrial polyps has been shown to increase pregnancy rates in intrauterine insemination cycles [4] and may decrease miscarriage rates in IVF cycles [5]. The high incidence of cavitory abnormalities in infertility patients and the potential improvements in pregnancy outcomes highlight the importance of a cavitory assessment for these patients. In addition to polyps, uterine synechiae and submucosal fibroids can be detected with these modalities.

The diagnosis of uterine adhesions or synechiae is difficult to make without uterine distension. A thickened endometrial stripe on routine ultrasound may suggest occurrence of synechia in the differential diagnosis. MRI may pick up synechiae as hypointense bands within the cavity. However, synechiae are best seen as areas of nonfilling inside the cavity on HSG or as bands of hyperechoic tissue within the cavity on SIS. While the occurrence of synechia may be strongly suspected on the basis of imaging studies, ultimately hysteroscopy is required for definitive diagnosis and treatment.

Currently, many patients may undergo both HSG and SIS during the course of an infertility evaluation. SIS allows cavity and myometrial assessment and HSG allows cavity and tubal patency assessment. Newer technologies provide the possibility of performing a single test that can assess the uterine cavity, uterine myometrium, and tubal patency. Three-dimensional dynamic magnetic resonance hysterosalpingography (3D dMR-HSG) offers similar tubal diagnostics as HSG with MRI-quality evaluation of the myometrium and other pelvic organs [6]. Another test uses CT technology to offer a similar assessment. Dubbed virtual hysterosalpingography (VHSG) or multi-slice computed tomography hysterosalpingography (MSCT-H), this technology offers similar information on tubal patency to that provided by HSG while providing superior information on the uterine cavity and myometrium [7,8]. These tests have the advantage of causing less patient discomfort and affording more diagnostic information in a single test. However, they are more expensive than either HSG or SIS.

Assessment of uterine leiomyoma is historically achieved with ultrasonography, although CT and MRI also offer detection of uterine fibroids. For intramural fibroids, transvaginal ultrasound offers good diagnostic capabilities. When a submucosal fibroid is suspected, SIS can characterize the size and cavity involvement. Recently, 3D ultrasound was found to have similar diagnostic capability to hysteroscopy. The advantage of 3D ultrasound over 2D imaging is a more accurate measurement of intramural versus submucosal involvement of the leiomyoma [9]. This information may be useful to the surgeon in determining whether to employ a hysteroscopic or an abdominal route to myomectomy.

MRI is superior to CT in imaging of soft tissue, as sensitive in identifying fibroids as TVUS, and is superior to TVUS for mapping fibroids, especially when they are large and multiple [10]. The signal intensity of T2- and T1-weighted images provides additional architectural information [11]. Low T2 signal intensity is associated with hyalinization, whereas increased T2 intensity is associated with edema and myxoid degeneration. Cystic degeneration lacks enhancement and has low T1 intensity with high T2 intensity. Hemorrhagic infarction can appear as a high-intensity T1 signal on the periphery of the lesion and a low-intensity T2 signal inside. Ultrasound remains the most cost-effective screening modality for uterine fibroids. When more information is needed on the location and architecture of a fibroid, MRI is an effective secondary imaging modality.

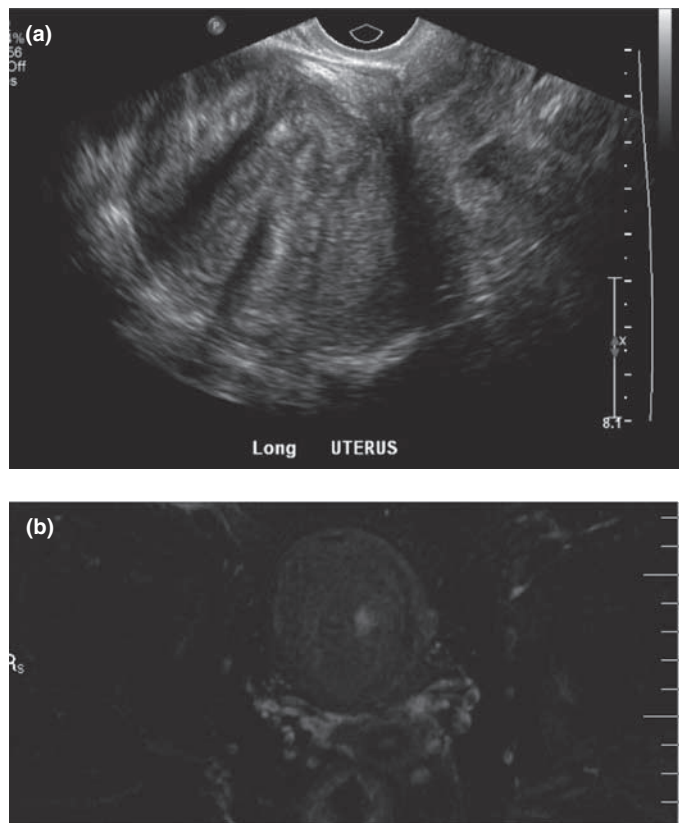


**Figure 1.3.** (a) Ultrasound shows the appearance of uterine leiomyoma. (b) MRI confirms the suspected diagnosis.

In Figures 1.3 and 1.4, various uterine imaging techniques are shown for a patient with hereditary leiomyomatosis and renal cell cancer (HLRCC), an autosomal dominant syndrome typified by renal cell carcinoma and uterine leiomyomas and an increased risk of leiomyosarcoma. Figure 1.3a shows a very typical appearance of a leiomyoma on ultrasound, with a heterogeneous swirling pattern in the tissue. On MRI, the lesion was confirmed to be a single and large uterine fibroid as suspected from ultrasound (Figure 1.3b). In HLRCC, the underlying disease is caused by mutations in the fumarate hydratase gene. This gene encodes for an enzyme in the Krebs cycle and affected cells show abnormalities in energy metabolism. Leiomyomas in HLRCC patients show significant uptake of fluorodeoxyglucose (FDG) on PET scan (Figure 1.4). This is in contrast to the majority of leiomyomas which show no FDG activity. Whether PET scan uptake of FDG has any predictive value for the behavior of fibroids is unknown.

In the management of uterine fibroids, radiologic technology is moving from the realm of diagnostics into the realm of treatment. Uterine artery embolization (UAE) is an interventional procedure wherein the uterine vessels are embolized. While it is an effective treatment for some women with menorrhagia, it is not recommended for patients desiring fertility and currently does not have a role in reproductive medicine. MRI-guided focused ultrasound surgery (MRgFUS) identifies

### Section 1: Imaging techniques

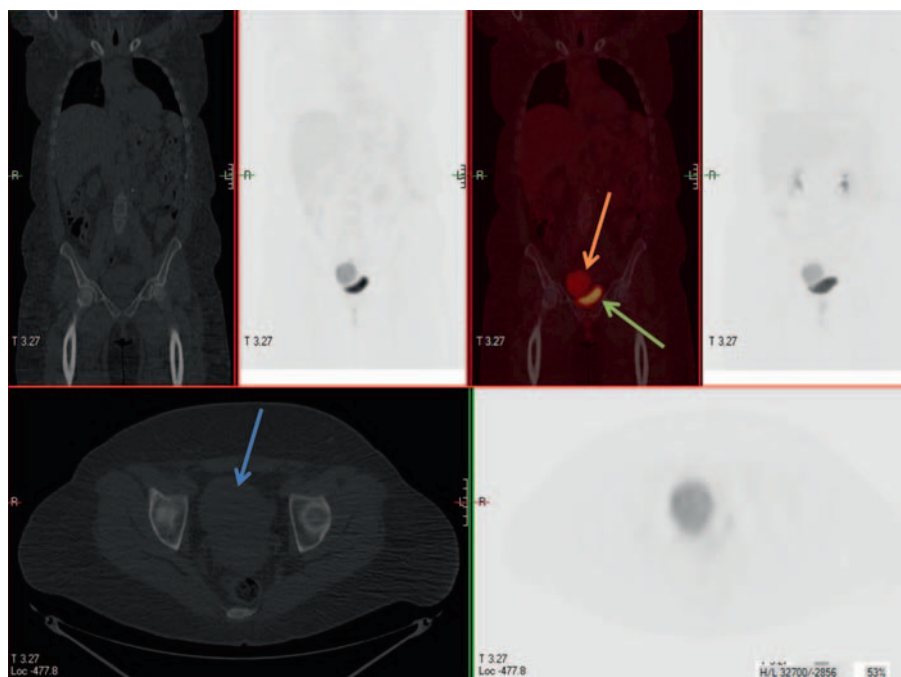


**Figure 1.4.** PET-CT images of the patient in Figure 3. CT shows the appearance of the fibroid (blue arrow) with less architectural information than the MRI in Figure 1.3. The fibroid shows significant uptake of FDG (orange arrow) and is distinct from the bladder (green arrow).

the fibroids with MRI and utilizes transabdominal ultrasound waves to cause thermoablation [12]. Two case reports have identified successful pregnancies after this treatment [13,14]. While this technology is still investigational, it may represent a viable alternative to the surgical risks and adhesion formation associated with abdominal myomectomy.

Adenomyosis is a cause of dysmenorrhea and menorrhagia. Recent data suggest that up to 90% of infertile women with endometriosis have concurrent adenomyosis [15]. Adenomyosis can be identified with either TVUS or MRI, although MRI is more accurate [16]. On ultrasound, adenomyosis appears as an asymmetry and thickening of the uterine walls. Adenomyosis is also suspected when a poorly defined, heterogeneous area is seen with either increased or decreased echogenicity [11]. On MRI, a diagnosis of adenomyosis is made with a thickened junctional zone on T2-weighted images or an area with low T1 and T2 signal intensity and indistinct margins [11]. MRI is the imaging of choice when differentiating between adenomyosis and leiomyosis, although diffuse adenomyosis may overlap with fibroids and become difficult to differentiate [17]. MRgFUS has been used to treat one patient with adenomyosis who subsequently had a successful pregnancy [13].

Müllerian anomalies are congenital defects in the development of the uterus and upper vagina. Suspicion of a müllerian anomaly typically arises in response to an abnormal screening test, such as HSG or ultrasound. While HSG and ultrasound are effective at defining normal anatomy, they lack specificity in diagnosing müllerian anomalies. For example, HSG may show a filling defect in the caudal midline of the uterus, but cannot definitively differentiate between a septum, bicornuate, or arcuate uterus. For definitive classification of a müllerian anomaly, MRI is typically indicated. The ability of this test to define soft



**Figure 1.5.** Transvaginal ultrasound shows two distinct and separate endometrial stripes approaching the uterine fundus.

tissue (such as endometrium versus myometrium) allows for accurate description of the anomaly.

Figures 1.5–1.10 show patients with congenital anomalies of the uterus. The first is an infertility patient thought to have a bicornuate uterus on routine screening transvaginal ultrasound (Figure 1.5). Routine 2D US can lack specificity if differentiating arcuate, bicornuate, and septated uteri. The diagnosis was confirmed with a 3D ultrasound (Figure 1.6), which provides a much better three-dimensional analysis of the uterus. MRI has historically been the gold standard radiologic test for uterine anomalies and combined laparoscopy and hysteroscopy the definitive test. Figures 1.7–1.10 show various images from patients with uterine septi both preoperatively and postoperatively. In the first patient, screening TVUS

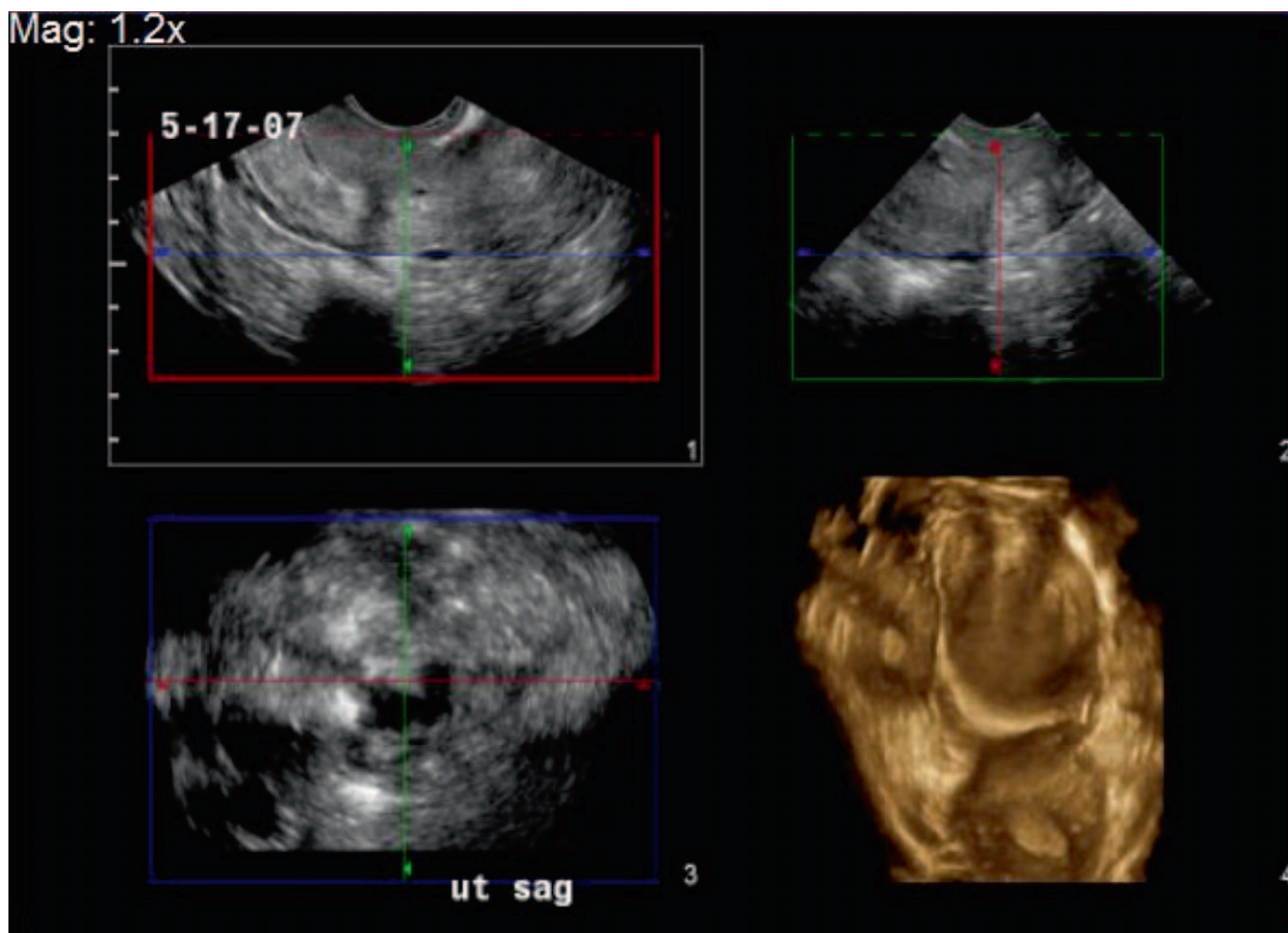


**Figure 1.6.** Multiplanar display of a septated uterus. Images displayed are sagittal, axial, coronal, and 3D surface rendering.

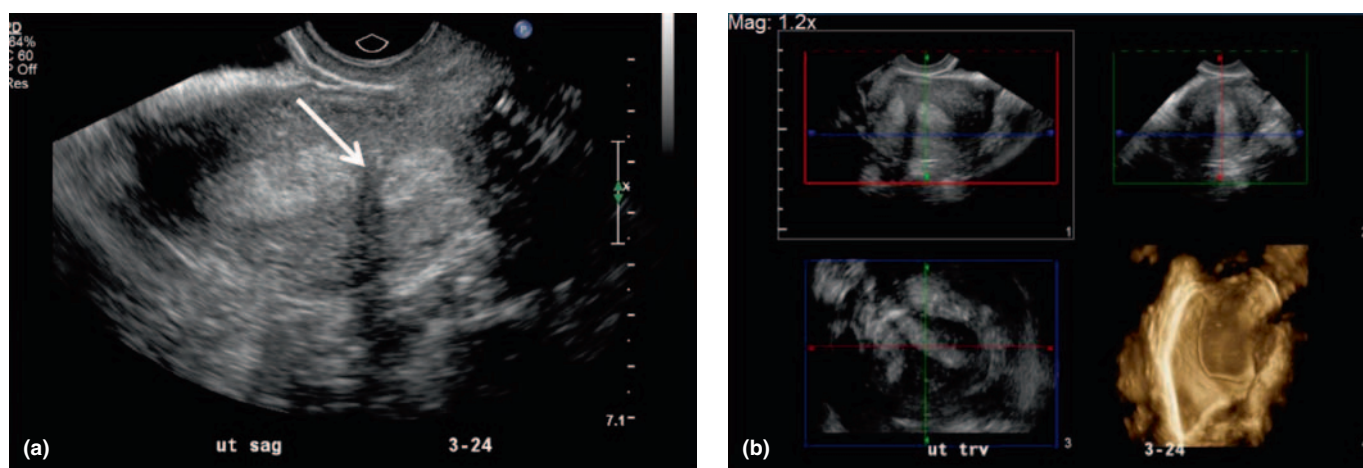


**Figure 1.7.** 2D and 3D TVUS views of a thick uterine septum. (a) 2D TVUS reviews a defect separating the endometrium (white arrow). This image alone cannot differentiate between septum, bicornuate, and arcuate uterus. (b) Multiplanar images (sagittal, axial, coronal, and 3D rendering) of the septum.

revealed a defect in the endometrium thought to represent a uterine septum (Figure 1.7a) and this was again confirmed with 3D US (Figure 1.7b). MRI further defined this very thick muscular septum (Figure 1.8a,b). Postoperative views of a different patient with a

septum in Figure 1.9 show persistence of the septum at the cervix with absence of the septum in the uterine cavity itself. Finally, an intraoperative saline infusion sonogram (Figure 1.10), confirms resection of the septum within the uterine cavity.

Section 1: Imaging techniques

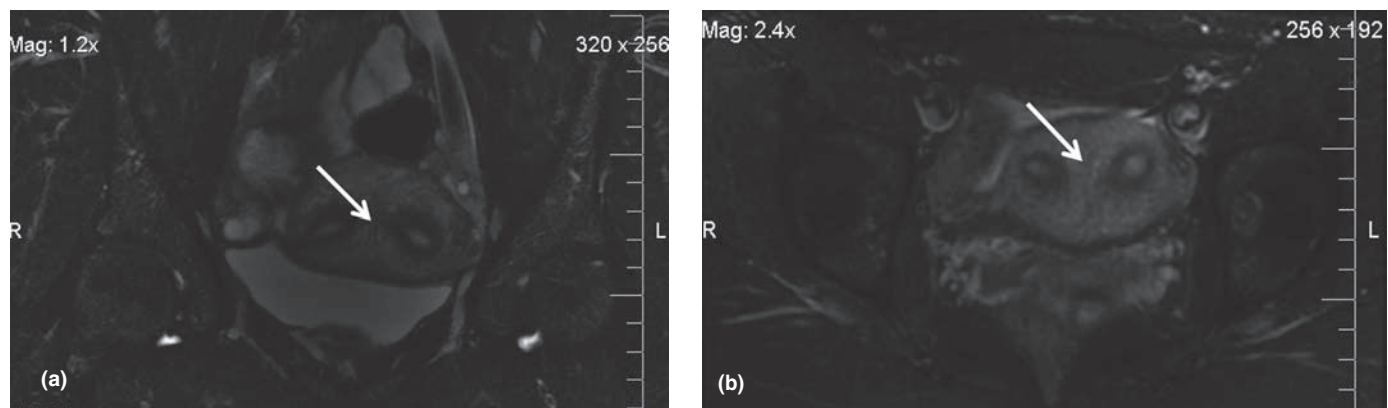


**Figure 1.8.** A coronal view (a) and axial view (b) by MRI of the thick muscular uterine septum (white arrows).

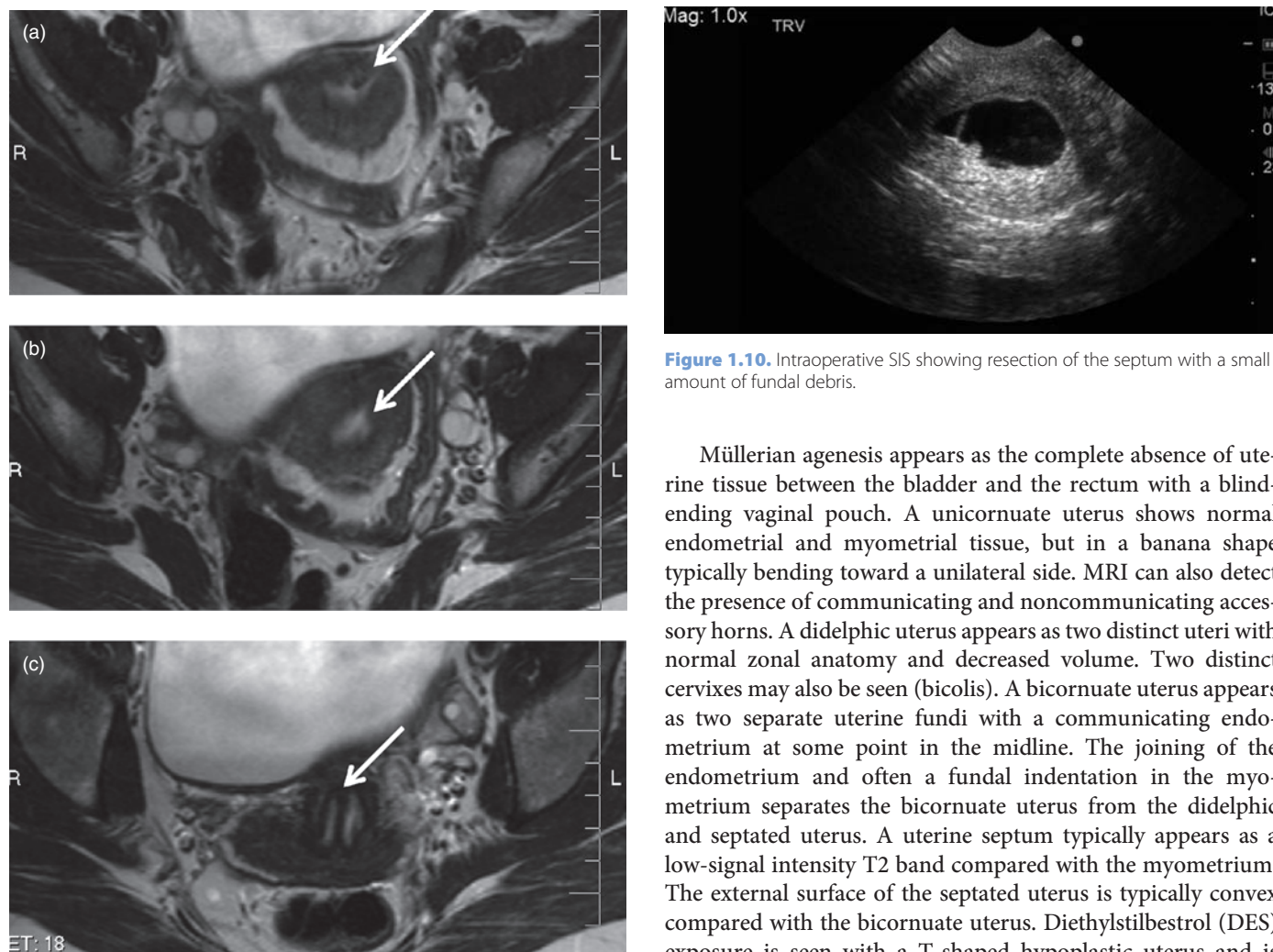


**Figure 1.9.** Three MRI T2-weighted axial views of the uterus from the fundus (a), mid-uterus (b), and the cervix (c). The patient had undergone resection of a uterine septum. The remaining portion of the septum at the fundus (top white arrow) is typical as the resection is often stopped prior to entry to the myometrium in an effort to avoid perforation. The middle arrow shows no evidence of septum in the main portion of the uterine cavity. The bottom white arrow shows persistence of the septum at the level of the cervix.

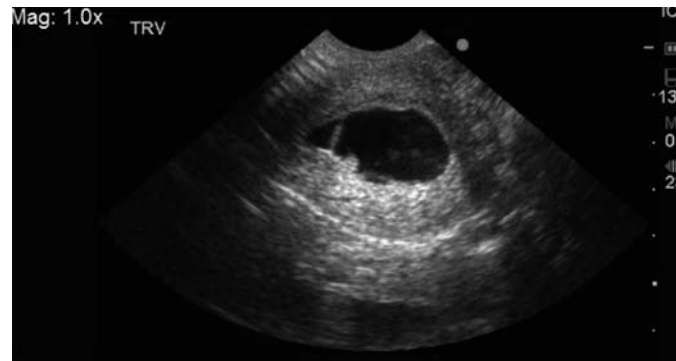


**Figure 1.10.** Intraoperative SIS showing resection of the septum with a small amount of fundal debris.

Müllerian agenesis appears as the complete absence of uterine tissue between the bladder and the rectum with a blind-ending vaginal pouch. A unicornuate uterus shows normal endometrial and myometrial tissue, but in a banana shape typically bending toward a unilateral side. MRI can also detect the presence of communicating and noncommunicating accessory horns. A didelphic uterus appears as two distinct uteri with normal zonal anatomy and decreased volume. Two distinct cervixes may also be seen (bicolis). A bicornuate uterus appears as two separate uterine fundi with a communicating endometrium at some point in the midline. The joining of the endometrium and often a fundal indentation in the myometrium separates the bicornuate uterus from the didelphic and septated uterus. A uterine septum typically appears as a low-signal intensity T2 band compared with the myometrium. The external surface of the septated uterus is typically convex compared with the bicornuate uterus. Diethylstilbestrol (DES) exposure is seen with a T-shaped hypoplastic uterus and is easily noted on both MRI and HSG. For evaluation of müllerian anomalies, MRI is currently the modality of choice [17]. As renal and skeletal anomalies can occur in conjunction with müllerian anomalies, additional imaging is also warranted.

Currently ultrasound plays a role in monitoring the uterus during ovarian stimulation and early pregnancy, although the role of uterine monitoring may be less important than ovarian

monitoring. It appears that the initial endometrial thickness is not predictive of IVF pregnancy outcomes but that the change in endometrial thickness on day 6 of gonadotropins is predictive of pregnancy rates [18].

After any form of ovarian stimulation or the use of assisted reproductive technology, it is incumbent upon the clinician to insure that an intrauterine pregnancy has resulted. In the presence of a positive serum or urine hCG (human chorionic gonadotropin) test, well-defined progression of ultrasound findings should ensue. Absence of these sonographic milestones in concert with aberrant hCG trends may suggest ectopic pregnancy or an abnormal uterine gestation. Early pregnancy is best assessed through transvaginal ultrasound. Imaging that utilizes ionizing radiation is unnecessary and is discouraged.

The first sign of intrauterine pregnancy is the gestational sac, a small hypoechoic area that can be detected at 2–3 mm. A small gestational sac is not diagnostic of intrauterine gestation, as ectopic pregnancy can be associated with an intrauterine pseudogestational sac. Gestational sac size should be measured in three dimensions and averaged to give a mean sac diameter (MSD). The next sonographic finding of a normal gestation is the appearance of the yolk sac, a hyperechoic ring within the gestation sac which should be visible with a MSD of 8 mm. When the MSD is 16 mm, the presence of an embryo with cardiac activity should be seen [19]. Transvaginal ultrasound will detect a singleton fetal pole when the hCG is between 1500 and 2000 (mIU/ml). The specific value should be determined individually at each institution, and is dependent upon the machines used and the experience of the sonographer. Finally, while there are many guidelines and milestones in use for early pregnancy ultrasonography, it should be emphasized that these are typically based upon singleton gestation data. In the USA in 2005, 37% of all live births from ART were multiple gestations [20]. Sonographic and hCG milestones for multiple gestations are not well established.

## Ovaries

The ovaries are paired organs suspended bilaterally to the uterus via the utero-ovarian ligaments and to the pelvic sidewall via the infundibulo-pelvic ligaments. The ovary itself is composed of germ cells, stromal cells, and epithelium. Antral follicles are visible as small cysts within the ovary. Stromal cells around the follicles secrete androgens and estrogens. Ovarian stroma appears heterogeneous and mildly hyperechoic on ultrasound, whereas follicles are hypoechoic.

Historically, the diagnosis of polycystic ovary syndrome (PCOS) was based upon ultrasound findings such as a “string of pearls” appearance of the antral follicles. The 2003 revised Rotterdam criteria for PCOS include the “presence of 12 or more follicles in each ovary measuring  $2 \pm 9$  mm in diameter, and/or increased ovarian volume ( $>10$  ml)” [21]. An assessment of ovarian follicles is best made with transvaginal ultrasound. A three-dimensional volumetric measurement can also be obtained easily with ultrasound. These ultrasound findings together with the clinical criteria of anovulation or oligo-ovulation

and hyperandrogenism define PCOS. While the ovarian measurements are important to the Rotterdam criteria, the clinical manifestations of PCOS remain the essential features of the disease.

Ultrasonography of the ovary also has a role in assisted reproductive technologies’ (ART) monitoring and prediction of success. Baseline characteristics and changes in follicle size during ovarian stimulation are readily measured via transvaginal ultrasound. Antral follicles are small hypoechoic structures within the ovary and typically measure between 2 and 10 mm. A basal count (BAFC) can be measured in the early follicular phase or after pituitary downregulation. Several studies suggest that the basal antral follicle count is predictive of ovarian response to gonadotropins and correlates with pregnancy rates [22,23]. In a meta-analysis by Hendriks et al., receiver operator curves showed basal antral follicle count (BAFC) as outperforming FSH in predicting poor response to ovarian stimulation [24]. Both tests performed poorly in predicting pregnancy. Ovarian volume also correlates with stimulation parameters and is predictive of cycle cancellation when  $<20$  mm [22]. Many ART programs employ TVUS ovarian monitoring in concert with serum estradiol levels to manage gonadotropin stimulation, hCG injection timing, and oocyte retrieval. Such monitoring gives knowledge of the number of growing follicles and their individual size.

In addition to ART monitoring, basal ovarian ultrasound is often assessed prior to any form of ovarian stimulation. Ovarian cysts may have a negative effect on ovarian stimulation and can occur in up to 18% of patients. In one study, patients with ovarian cysts greater than 10 mm ovulated 81% of the time on clomiphene citrate as compared with 97% in the group without cysts [25]. A screening evaluation of the ovary for cysts over 1 cm may be indicated before ovarian stimulation.

It should be noted that the role of ovarian imaging is much broader in the context of gynecology and oncology than presented here. In general, the first-line imaging role for any suspected ovarian mass should be transvaginal ultrasound. Ultrasound provides a superior evaluation and characterization of the ovaries and is less expensive than other modalities. However, there are scenarios where other modalities, such as CT or MRI, provide important information for the oncologist and gynecologist.

## Fallopian tubes

The fallopian tubes serve as a hollow conduit to transport oocytes from the peritoneal cavity to the uterus. The tubes are typically 10–14 cm in length and divided into regions: interstitial, isthmic, ampullary, infundibulum and ending in fimbria. In reproductive medicine, imaging of the tubes is typically limited to evaluation of patency and distortion of normal anatomy, as in hydrosalpinges and salpingitis isthmica nodosum.

Evaluation of tubal patency is a routine step in the infertility evaluation. This is most easily performed with hysterosalpingography (HSG). HSG provides a series of fluoroscopic x-ray images to show the filling of the fallopian tubes and the passage of contrast material into the peritoneal cavity. Passage of

## Section 1: Imaging techniques

contrast medium confirms patency of the tubes. Filling of the tube with contrast but without spillage indicates distal tubal disease. Filling of the uterus but without contrast fill of the fallopian tube indicates either proximal disease or tubal spasm. Premedication with antispasmodic agents prior to the procedure may reduce tubal spasm. HSG not only provides information on tubal patency, but can also assess the tubes for disease. Salpingitis isthmica nodosa (SIN) can appear as a honeycomb appearance of the contrast. Other abnormalities which have been detected by HSG include müllerian anomalies, uterine cancer, leiomyoma, DES exposure, adenomyosis, synechia, and tubal polyps [26].

As mentioned under uterine imaging, research has evaluated CT and MRI technology for combined uterine and tubal patency studies. The early data on these studies suggest it is effective for tubal imaging. However, routine use of this technology is limited by its cost.

Ultrasonographic evaluation of the fallopian tubes is often difficult in the absence of significant pathology. The exception to this is for hydrosalpinges. If the HSG shows a dilated tube, this could be secondary to distal obstruction with iatrogenic tubal contrast filling or due to hydrosalpinges. For patients who will undergo IVF, this distinction is important. On ultrasound, a hydrosalpinx will appear as a “sausage-shaped” hypoechoic area between the uterine cornua and the ovary. In a meta-analysis, Zeyneloglu et al. showed that patients with hydrosalpinges had 50% lower implantation rates and ongoing pregnancy rates than patients without hydrosalpinges [27]. For patients undergoing IVF, ultrasonography of the fallopian tubes to assess for hydrosalpinges is warranted.

### Lower genital tract

The lower genital tract consists of the structures of the vulva and the lower portion of the vagina. The vulva contains the mons pubis, labia majorum and minorum, hymen, urethra, clitoris, vestibular bulbs, and Skene’s and Bartholin’s glands. The mons pubis is a fatty eminence overlying the symphysis pubis. The hymen is a thin membrane of squamous epithelium at the vaginal opening that is present in varying degrees in childhood. The clitoris is located at the superior aspect of the vestibule and is composed of vascular channels that function as erectile tissue. The urethra is also located in the superior vestibule, located inferior and internal to the clitoris. It is typically 3–5 cm in length and serves as a conduit of urine from the bladder to the outside of the body. Located adjacent to the distal urethra are the Skene’s glands (para-urethral glands), which are the homologue to the male prostate. Bartholin’s ducts open between the hymen and the labia minora and serve to drain the Bartholin’s glands, which are located posterolateral to the vagina near the introitus.

The lower genital tract is separate from the remainder of the female reproductive tract embryologically. The clitoris develops from the genital tubercle, the labium from the genital folds, and the vestibule from the urogenital sinus. The urogenital sinus must meet with the müllerian ducts and undergo a process of

fusion, elongation, and canalization. Whereas the gynecologist and oncologist may have numerous diseases of the lower genital tract to evaluate and treat, the majority of consultations in reproductive medicine involve improper fusion of the müllerian duct and urogenital sinus.

The most common clinical scenario involving lower genital tract imaging for the reproductive clinician entails the imperforate hymen. On examination, the clinician encounters a blocked vagina, anywhere from the level of the hymen up to the uterus. In most cases the location of the obstructing tissue and findings on physical examination often differentiate the imperforate hymen from the transverse vaginal septum, although addition imaging may be needed. If physical examination alone is insufficient, ultrasound can determine whether the uterus is present and evaluate for hematocolpos. Ultimately, MRI may be necessary in complex cases or those involving müllerian anomalies. CT scans can evaluate Skene’s duct cysts and ureteral diverticula. In reproductive medicine, physical examination is typically adequate for lower urinary tract evaluation.

### Pituitary

The pituitary gland is a roundish organ located at the base of the skull in the sella turcica. The pituitary is located inferior to the hypothalamus and the optic chiasm, which it may compress when it enlarges. The anterior pituitary secretes hormones in response to pituitary release hormones. The posterior pituitary consists of hypothalamic neurons which release antidiuretic hormone and oxytocin.

Pituitary imaging is mostly performed in reproductive medicine for the infertile patient with persistently elevated prolactin levels or with levels over 100 ng/ml. Although prolactin levels correlate with the size of pituitary adenomas, macroadenomas may present with only moderate elevations in prolactin [28]. MRI imaging appears to be superior to CT evaluation and has replaced the historical coned-down radiographic view for imaging of the sella turcica [29]. Microadenomas by definition are less than 10 mm in maximal dimension whereas macroadenomas are 10 mm or greater. Adenomas are identified as a lower-intensity T1-weighted signal on MRI [11]. Newer dynamic MRI studies are performed with IV contrast and show greater sensitivity in detecting microadenomas. In these studies the normal pituitary enhances, while microadenomas show only weak enhancement.

### Peritoneum

Imaging is rarely performed in reproductive medicine specifically to evaluate for peritoneal disease. Laparoscopy is considered the gold standard for diagnosis of peritoneal processes such as endometriosis. CT has been shown to be effective in evaluation for peritoneal malignancy [30]. For evaluation of deep endometriosis, including the peritoneal surfaces, MRI has been shown to have high sensitivity and specificity [31]. The ability of these tests to detect very small areas of endometriosis and their broad clinical utility is uncertain at present.

## Summary

Imaging techniques play a key role in the evaluation of reproductive diseases and an increasingly prominent role in the treatment of such diseases. The possible applications of newer technologies are promising. Three-dimensional dynamic magnetic resonance hysterosalpingography (3D dMR-HSG) and multislice computed tomography hysterosalpingography (MSCT-H) can offer evaluation of tubal patency with superior imaging of the uterine, tubal, and ovarian anatomy. Positron emission tomography (PET) and computed tomography (CT) scans can be overlaid to provide detailed anatomic information correlated with metabolic activity. Such testing shows increased activity in certain types of fibroids [32]. In addition, PET scans show variation in the uterus and the ovaries during different times of the menstrual cycle. What clinical relevance this has warrants investigation. The future applications of newer imaging modalities are numerous for reproductive imaging, though cost will continue to be a factor.

## References

- Rindfleisch W. Darstellung des Cavum uteri. *Klin Wochenschr* 1910; **4**: 780.
- Tur-Kaspa I, Gal M, Hartman M, Hartman J, Hartman A. A prospective evaluation of uterine abnormalities by saline infusion sonohysterography in 1,009 women with infertility or abnormal uterine bleeding. *Fertil Steril* 2006; **86**: 1731–5.
- Keleci S, Kaya E, Alan E, Alan Y, Bilge U, Mollamahmutoglu L. Comparison of transvaginal sonography, saline infusion sonography, and office hysteroscopy in reproductive-aged women with or without abnormal uterine bleeding. *Fertil Steril* 2005; **84**: 682–6.
- Perez-Medina T, Bajo-Arenas J, Salazar F, et al. Endometrial polyps and their implication in the pregnancy rates of patients undergoing intrauterine insemination: a prospective, randomized study. *Hum Reprod* 2005; **20**: 1632–5.
- Lass A, Williams G, Abusheikha N, Brinsden P. The effect of endometrial polyps on outcomes of in vitro fertilization (IVF) cycles. *J Assist Reprod Genet* 1999; **16**: 410–15.
- Unterweger M, Geyter CD, Fröhlich FM, Bongartz G, Wiesner W. Three-dimensional dynamic MR-hysterosalpingography; a new, low invasive, radiation-free and less painful radiological approach to female infertility. *Hum Reprod* 2002; **12**: 3138–41.
- Carrascosa M, Baronio M, Capuñay C, López EM, Sueldo C, Papier S. Clinical use of 64-row multislice computed tomography hysterosalpingography in the evaluation of female factor infertility. *Fertil Steril* 2008; **90**: 1953–8.
- Baronio JM, Carrascosa P, Ulla M, Papier S, Borghi M, Sueldo C. Virtual hysterosalpingography: A novel painless technique for the study of the female reproductive tract in infertile patients. *Fertil Steril* 2006; **86**: s51
- Salim R, Lee C, Davies A, Jolaoso B, Ofuasia E, Jurkovic D. A comparative study of three-dimensional saline infusion sonohysterography and diagnostic hysteroscopy for the classification of submucous fibroids. *Hum Reprod* 2005; **20**: 253–7
- Dueholm M, Lundorf E, Hansen ES, Ledertoug S, Olesen F. Accuracy of magnetic resonance imaging and transvaginal ultrasonography in the diagnosis, mapping, and measurement of uterine myomas. *Am J Obstet Gynecol* 2002; **186**: 409–15
- Imaoka I, Wada A, Matsuo M, Yoshida M, Kitagaki H, Sugimura K. Imaging of disorders associated with female infertility: use in diagnosis, treatment, and management. *RadioGraphics* 2003; **23**: 1401–21
- Stewart EA, Rabinovici J, Tempany CM, et al. Clinical outcomes of focused ultrasound surgery for the treatment of uterine fibroids. *Fertil Steril* 2006; **85**: 22–9.
- Rabinovici J, Inbar Y, Eylon SC, Schiff E, Hananel A, Freundlich D. Pregnancy and live birth after focused ultrasound surgery for symptomatic focal adenomyosis: a case report. *Hum Reprod* 2006; **21**: 1255–9.
- Hanstede MF, Tempany CM, Stewart EA. Focused ultrasound surgery of intramural leiomyomas may facilitate fertility: A case report. *Fertil Steril* 2007; **88**: 497.e5–7.
- Kunz G, Beil D, Huppert P, Noe M, Kissler S, Leyendecker G. Adenomyosis in endometriosis – prevalence and impact on fertility. Evidence from magnetic resonance imaging. *Hum Reprod* 2005; **20**: 2309–16.
- Ascher SM, Arnold LL, Patt RH, et al. Adenomyosis: prospective comparison of MR imaging and transvaginal sonography. *Radiology* 1994; **190**: 803–6.
- Reinhold C. Pelvic MR imaging in infertility and recurrent pregnancy loss. *International Congress Series* 2004; **1266**: 401–8.
- McWilliams GD, Frattarelli JL. Changes in measured endometrial thickness predict in vitro fertilization success. *Fertil Steril* 2007; **88**: 74–8.
- Levi CS, Lyons EA, Lindsay DJ. Early diagnosis of non-viable pregnancy with transvaginal ultrasound. *Radiology*. **167**: 383–5.
- Centers for Disease Control and Prevention, American Society for Reproductive Medicine, Society for Assisted Reproductive Technology. *2005 Assisted Reproductive Technology Success Rates: National Summary and Fertility Clinic Reports*. Atlanta GA: Centers for Disease Control and Prevention; 2007.
- The Rotterdam ESHRE/ASRM-sponsored PCOS consensus workshop group. Revised 2003 consensus on diagnostic criteria and longterm health risks related to polycystic ovary syndrome (PCOS). *Hum Reprod* 2004; **19**: 41–7.
- Frattarelli JL, Lauria-Costa DF, Miller BT, Bergh PA, Scott RT. Basal antral follicle number and mean ovarian diameter predict cycle cancellation and ovarian responsiveness in assisted reproductive technology cycles. *Fertil Steril* 2000; **74**: 512–17.
- Frattarelli JL, Levi AJ, Miller BT, Segars JH. A prospective assessment of the predictive value of basal antral follicles in in vitro fertilization cycles. *Fertil Steril* 2003; **80**: 350–5.
- Hendriks DJ, Mol BJ, Bancsi LF, Velde DE, Broekmans FJ. Antral follicle count in the prediction of poor ovarian response and pregnancy after in vitro fertilization: a meta-analysis and comparison with basal follicle stimulating

### Section 1: Imaging techniques

- hormone level. *Fertil Steril* 2005; **83**: 291–301.
25. Csokmay JM, Frattarelli JL. Basal ovarian cysts and clomiphene citrate ovulation induction cycles. *Obstet Gynecol* 2006; **107**: 1292–6.
26. Baramki TA. Hysterosalpingography. *Fertil Steril* 2005; **83**: 1595–606.
27. Zeyneloglu HB, Arici A, Olive DL. Adverse effects of hydrosalpinx on pregnancy rates after in vitro fertilization-embryo transfer. *Fertil Steril* 1998; **70**: 492–9.
28. Bayrak A, Saadat P, Mor E, Chong L, Paulson JP, Sokol RZ. Pituitary imaging is indicated for the evaluation of hyperprolactinemia. *Fertil Steril* 2005; **84**: 181–5.
29. Kulkarni MV, Lee KF, McArdle CB, Yeakley JW, Haar FL. 1.5-T MR imaging of pituitary microadenomas: technical considerations and CT correlation. *Am J Neuroradiol* 1987; **9**: 5–11.
30. Shaw MS, Healy JC, Reznik RH. Imaging the peritoneum for malignant processes. *Imaging*. 2000; **12**: 21–33.
31. Bazot M, Darai E, Hourani R, et al. Deep pelvic endometriosis: MR imaging for diagnosis and prediction of extension of disease. *Radiology* 2004; **232**: 379–89.
32. Blake MA, Singh A, Setty BN, et al. Pearls and pitfalls in interpretation of abdominal and pelvic PET-CT. *RadioGraphics* 2006; **26**: 1335–53.